2019 SECED Conference
Earthquake risk and engineering towards a resilient world
9-10 September 2019, Greenwich, London

The Role of Ageing and Corrosion Damage in the Relevance of Seismic Assessment

Nicolas EL JOUKHADAR[1], Konstantinos TSIOTSIAS[1], Stavroula PANTAZOPOULOU[2]

Abstract: *Methods of seismic assessment of RC that find their way to practical application (see for example Eurocode 8-III) are calculation-intensive requiring extensive information about the layout and amount of reinforcement, in order to evaluate the dependable deformation capacity of the structural members to predict the performance in a future seismic hazard. Very little reference is made by the Assessment Guidelines to the condition of reinforcing materials, and the effect this may have on residual capacity, hierarchy of likely failure modes and the resulting implications on seismic performance. In fact, this is not a straightforward problem, as it induces an important level of uncertainty on the rather complex problem of calculating the response of poorly detailed reinforced concrete members under cyclic load reversals. This objective is pursued in the present study. The deprecating effects of corrosion-affected reinforcement on the mechanical response of a sample reinforced concrete element with substandard detailing representative of old practices and subjected to either moderate carbonation, or to cyclical chloride exposure for a period of 50 years (a sample of conditions in coastal urban areas build in the 70's) is the reference case study. The column is examined under cyclic load reversals simulating low, moderate and intense seismic activity. The performance, expressed in terms of shear vs drift capacity is introduced in the available methodologies of rapid assessment of reinforced concrete structures showcasing the limitations and uncertainties of the existing state of the art in the field of seismic assessment of existing structures.*

Introduction

Seismic Assessment codes have evolved in terms of the detailed information required in order to evaluate the available resistance of existing structures built in the past and still used today. This density of needed information pertains to the actual geometric details and material properties of the structure, and the need to account in a realistic manner of the degraded behaviour of the individual members in modelling and calculating the structural response; the level of confidence in the results is controlled through the so-called knowledge level, to the extent of material sampling conducted as part of the preliminary phase of the assessment. Nevertheless, once a material residual strength is determined, the way that the integrity of reinforcement and concrete is reflected in the analysis used to conduct the assessment is left upon the judgment of the engineer – no specific guidance is given regarding the way the design expressions for strength and deformation capacity of reinforced concrete members ought to be used when the actual reinforcement areas and arrangement have been compromised from their nominal values. This is a topic of great priority in coastal or urban regions of Europe and North America, where infrastructure and building development occurred in the post-war era, with structures today counting several decades of service life.

Seismic response of old structures may be hampered by bad practices, brittle design, or lack of any design of the original construction; but equally important is the damage accumulation that has occurred over the years of service. The circumstances that represent the condition of an assessed structural member are summarized in Table 1.

Clearly, the assessment should account for the additional implications of old age apart from the poor detailing in the era of construction of older structures; both the reinforcement ratios and material strengths, such as percentages of longitudinal, transverse and confining reinforcement, and reinforcement yield strengths, should be adjusted to account for the losses inflicted by environmental exposure.

[1] PhD Student, York University, Toronto, Canada, nicolasj@yorku.ca / kostasts@yorku.ca
[2] Professor of Civil Engineering, York University, Toronto, Canada.

Table 1: Compromised conditions of structural members in older construction

Initially poor material quality at the time of construction	Degradation of materials due to ageing and corrosion (e.g. embrittlement of concrete due to carbonation and loss of steel material strength and deformation capacity),
Inadequate sizes of members or member details (e.g. bar cover) due to underestimation of the seismic demands at the time of original design (if such exists) or due to poor construction practices,	Deprecation of existing geometric details due to damage (e.g. cover delamination due to corrosion)
Sparsely spaced transverse reinforcement	Corroded stirrups that have fractured
Small bar Sections	Reduced bar sections due to corrosion
Smooth Reinforcement – low bond	Loss of ribs due to corrosion – effect on bond

Effect of Corrosion of reinforcement.

Corrosion products exert bursting pressures on the concrete cover which in turn lead to cracking or spalling and further acceleration of the corrosion process. From the point of view of Seismic Assessment, corrosion is a deprecating mechanism that materially affects the seismic resistance of a structural member: in this regard it should integrally embedded in the procedures for asset assessment, particularly where ductility which relies on the strain capacity of the reinforcement is the assessment objective.

Based on collected experimental evidence, corrosion effects a significant decrease in ductility, yielding and ultimate tensile strength of reinforcing bars (Almusallam, 2001; Du, Clark and Chan, 2005; Apostolopoulos, 2007; Apostolopoulos and Papadakis, 2008; Zhang et al., 2012; François, Khan and Dang, 2013; Zhu and François, 2014; Fernandez, Bairán and Marí, 2015; Lu et al., 2016). Figures 1 – 3 plot the evidence extracted from the published tests collected in a database: yield strength $F_{y(\%red)}$, ultimate strength $F_{u(\%red)}$ and ultimate elongation $\varepsilon_{max(\%red)}$ of corroded bars all degrade with increasing amount of average steel mass loss (x is the mass loss percent). Their values follow the trends quantified by Eqns. (1) – (3).

$$F_{y(\%red)} = F_y \cdot (1-1.08 \cdot x) \quad (1)$$

$$F_{u(\%red)} = F_u \cdot (1-1.15 \cdot x) \quad (2)$$

$$\varepsilon_{max(\%red)} = \varepsilon_{max} \cdot (1-4 \cdot x) \quad (3)$$

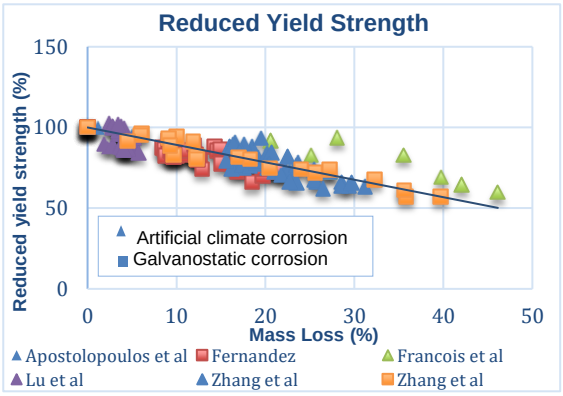

Figure 1 Reduced Yield Strength

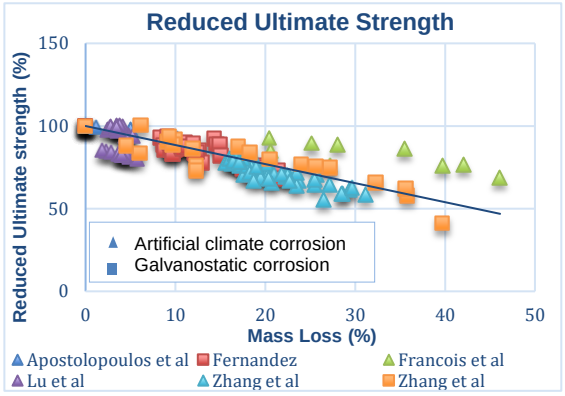

Figure 2 Reduced Ultimate Strength

It is noteworthy that the effect of corrosion on the ductility of steel is much more severe than the effect on the bar's strength. A decrease in yield and ultimate strength of up to 50% was observed for mass loss values, as high as x=45%, whereas the reduction in ductility observed was up to 80% for mass loss as low as 20%. Corrosion was investigated through various experimental setups: bars were tested either bare or embedded in concrete, while the oxidation process was accelerated either by manipulating the temperature and relative humidity through simultaneously inducing a salt fog, or by applying an impressed current. The variation in the aforementioned

experimental procedures is decidedly the major cause behind the dispersion in the test results. Of equal importance was the distinction of corrosion losses due to pitting and uniform corrosion. Pitting losses have a more drastic effect on the strength reduction of the bars than uniform losses.

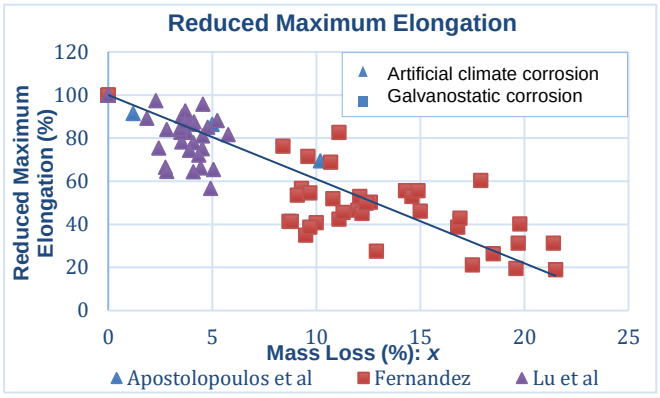

Figure 1 Reduced Maximum Elongation

Analysis of Corroded Columns

The assessment procedure for seismic resistance of structural members is conducted using two criteria as described in the study by (Pardalopoulos et al, 2017); these refer to the deformation demand in terms of relative drift ratio, θ_d, at peak response, and the available strength of the individual member at the attainment of the drift demand. Drift demand is a function of the structural period in the fundamental translational mode of vibration, $T_1(s)$, the design Spectral acceleration $S_a(T_1)$ and corresponding spectral displacement $S_d(T_1)=T_1^2 S_a(T_1)/4\pi^2$, and the layout of the structural system which controls the localization of deformation demands, which is quantified by the difference in the relative coordinates in the ends *i* and *j* of the member in the fundamental mode of vibration Φ of the structure: i.e., Φ_i-Φ_j.

To preclude failure the drift capacity of the member, θ_c, should exceed the demand, θ_d. Term θ_c is defined as the drift ratio beyond which the resistance envelope of the structural member subjected to lateral displacement reversals experiences severe degradation (the convention is to use the value corresponding to a post peak residual resistance equal to 85% of the strength). Several experiments have been conducted to study the effects of reinforcement corrosion on the strength and drift capacity of structural components. Major concerns are loss of bar area, embrittlement of the reinforcement and concrete, and degradation of bond strength between steel and concrete due to accumulation of rust (Almusallam et al., 1996; Mangat and Elgarf, 1999; Stanish et al. 1999; Tastani and Pantazopoulou, 2007; Zhao et al., 2013). The tests conclusively illustrate that both response indices are severely impacted; most importantly, the sequence of failure modes is often drastically affected, with members originally designed for flexure to be eventually failing by shear or in the anchorages/lap splices as a result of disproportional reduction of the stirrup bar area or of bar ribs (Tastani and Pantazopoulou 2005).

Database of published test specimens

A database of tests conducted under cyclic displacement reversals simulating earthquake effects on corroded columns was assembled (Appendix 1). Prior to testing, the columns had been corroded to various degrees of mass loss by accelerated corrosion. The acquired data was used to provide a thorough understanding of the mechanical effects of corrosion on columns as corrosion propagates, specifically in order to quantify the degradation in strength and ultimate drift capacity. The following studies were used in the database (Li et al., 2009; Ma at al., 2012; Meda *et al.*, 2014; Yang *et al.*, 2016; Yuan et al., 2017; Li *et al.*, 2018; Liu and Li, 2018; Rajput and Sharma, 2018; Vu and Li, 2018; Apostolopoulos et al., 2019)

Data Analysis

Columns were divided into two groups according with the magnitude of statically applied, overbearing axial load, *N*: this is quantified as a normalized ratio ($v=N/A_g f_c'$). Thus, Group #1 comprised columns with an axial load ratio $0 \le v \le 0.2$ (i.e. lightly loaded), whereas Group #2 comprised columns bearing a significant amount of axial load acting ($0.2 \le v \le 0.4$). In assessing their performance for the needs of the present study, parameters studied for the two groups were:

1) the ultimate drift capacity, θ_u, of the columns when rupture of the column's longitudinal bars occurred, 2) the lateral resistance $V_{cor}(\theta)$ of the columns at drift ratios equal to, θ=0.5% (at about yielding of longitudinal reinforcement), θ=1% and θ=2% (at approximate rotational ductilities, μ_θ, equal to 2 and 4, respectively).

Results are plotted in Fig. 4-7 where response indices are normalized with respect to their uncorroded counterpart: Figure 4 plots the percent reduction in ultimate drift capacity of specimen groups 1 and 2 against the reported mass loss ratio, x (black and orange points correspond to specimens of group #1 and #2 respectively; the trend lines bear the same colour code for easy reference).

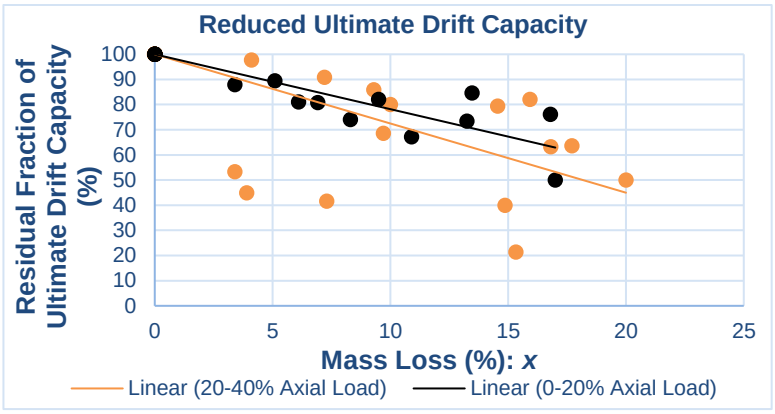

Figure 2 Reduction in the Ultimate Drift Capacities of groups 1 & 2

The steeper trend represents the reduced ultimate drift capacity of group #2, while the shallower represents that of group #1. These trends are approximated by the following equations for the reduced drift capacity $\Delta_{u,cor}$ given with reference to the uncorroded value $\Delta_{u,o}$ as a function of the steel mass loss percent (subscripts 1 and 2 correspond to the two groups):

$$\Delta_{u,cor,1} = \Delta_{u,o,1} \cdot (1-2.2 \cdot x) \quad (4)$$

$$\Delta_{u,cor,2} = \Delta_{u,o,2} \cdot (1-2.75 \cdot x) \quad (5)$$

It is observed that the deteriorating effect of corrosion on the ultimate drift capacity is greater on group # 2 columns, particularly in cases with a higher mass loss. Figures 5, 6 and 7 plot the normalized lateral load capacity of the columns, $V_{u,cor}$, at lateral drift ratios of 0.5%, 1% and 2% respectively (normalization is done with respect to the corresponding uncorroded strength, V_u). For drift ratio equal to 0.5% (approximately onset of yielding), both groups of specimens experience a mild reduction in resistance, with the normalized capacity ratio reaching approximately the value of 90% (on average) for mass losses as high as 20%. It could be argued that no significant decrease in strength is noticeable at this level of drift ratio. For 1% drift, the trends in the values of normalized lateral load resistance became steeper as compared to the 0.5% drift. A target value of 90% in normalized lateral strength occurred at a value of

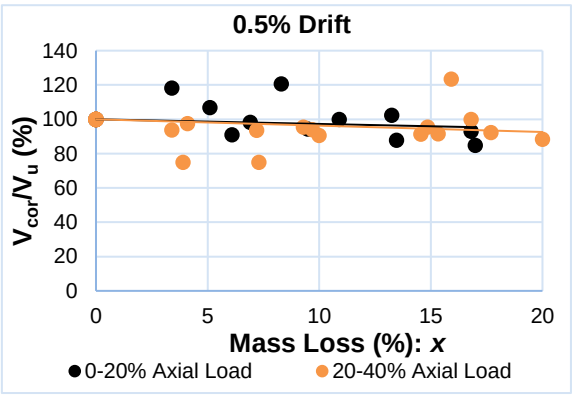

Figure 4 Reduction in Lateral Load Capacity at 0.5% Drift

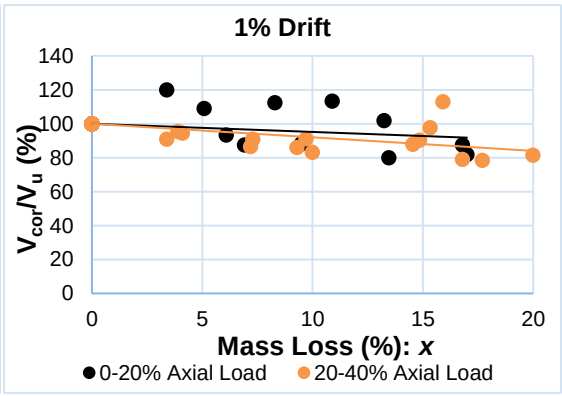

Figure 3 Reduction in Lateral Load Capacity at 1% Drift

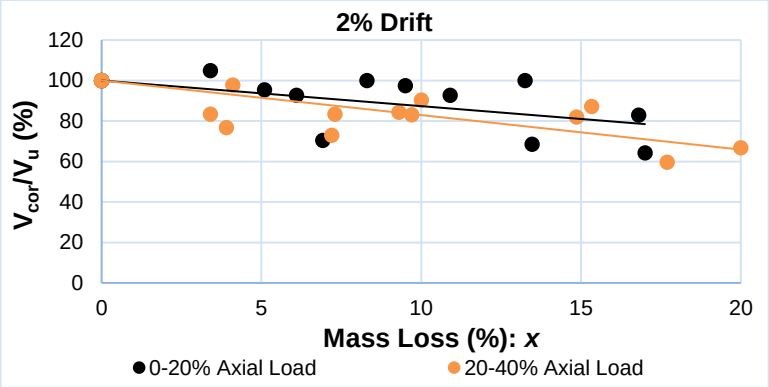

Figure 5 Reduction in Lateral Strength Capacity at 2% Drift

x=17% from group #1 columns, whereas at residual strength for group #1, at 17% mass loss, and 80% residual load for group #2, at 20% mass loss, and the gap between groups #1 and #2 became more evident. At 2% drift, the reduction in lateral resistance is more evident. Group #1 reaches 80% of residual strength at 17% of mass loss whereas group #2 reaches around 65% of resistance ratio at 20% mass loss.

A parametric equation was formulated to quantify the residual lateral resistance of the columns as a function of the mass loss and the drift demand. Equations (6) and (7) describe the observed trends for groups #1 and #2, respectively:

$$V_{cor} = V_u \cdot (1-0.005 \cdot \theta \cdot x) \quad (6)$$

$$V_{cor} = V_u \cdot (1-0.008 \cdot \theta \cdot x) \quad (7)$$

where V_{cor} is the lateral resistance of the corroded column at a given level of lateral drift, θ, and V_u is the corresponding resistance of the reference uncorroded column with identical loading and reinforcing details. Parameter x represents the mass loss percentage. Note that the reduction in lateral strength is directly proportional to the reduction in ultimate tensile strength of corroded bars and that the reduced ultimate drift capacity is directly proportional to the reduced maximum elongation of corroded bars owing to the fact that most studied columns failed in flexure instead of shear or anchorage slip.

Discrepancies in data are noted between specimens experiencing similar mass losses: this could be attributed to the different test setups, shear reinforcement arrangement and to the current density used in the accelerated corrosion process. Values of current densities ranged from 200 μA/cm^2 to 5000 μA/cm^2 which would yield different corrosive products with different densities of oxides. The difference in corrosive products' densities result in significantly different bond strengths and cracking in the concrete cover (Alonso *et al.*, 1998; El Maaddawy and Soudki, 2003). But the overall behavioural trend of the columns enables us to formulate an expression that helps us assess existing corroded structures.

Lateral Load Resistance Curve of Corroded Columns: Modelling with F.E.

To explore and illustrate the effects of corrosion on lateral load resistance, four columns taken from (Vu and Li, 2018) with an axial load ratio *v=10%* were modelled using the Finite Element platform ATENA (Cervenka Consulting, 2007). Details with regards to the specimens considered (U1, C1, C2, C3) are listed in the Appendix.

Material Properties

Concrete material model implemented was "3D Nonlinear Cementitious2", where the biaxial strength failure envelope under plane stress is specified as input. The nonlinearity in behaviour of concrete in the triaxial stress state is defined by an effective uniaxial stress based on the corresponding uniaxial strain in principal directions. The material was assigned the reported properties for the Modulus of elasticity of concrete, E_c, concrete compressive strength f_c', and the tensile strength ft. The Specific Fracture Energy was taken equal to: $G_f = 7.01\ E\text{-}5\ MN/m$, tension stiffening coefficient $C_{ts}=0.1$ and the unloading factor=0.01. Default values were used for the other parameters as per the ATENA manual. Reinforcing bars were modelled as truss elements using the "Cyclic Reinforcement" having a bilinear with hardening type behaviour. Input properties

were, the steel modulus E_s, yield stress f_y, ultimate stress f_u, and maximum (rupture) strain ε_{lim}. Reinforcement to concrete bond was calculated according with the FIB model code 2010: each of the four specimens considered had a different bond strength where U1 denotes the case with the highest and C3 the lowest bond strength. Only one shear span was modelled for each column (i.e. half the height of columns with fixity at top and bottom) representing them in the computer model as laterally swaying cantilevers. Loading plates were used to apply both lateral forces and axial forces. These auxiliary elements were assigned "3D Elastic Isotropic" material to enable more uniform spreading of the load in the contact surfaces and avoid local convergence problems.

Macro-Elements, Reinforcement and Solution Parameters

Meshing refers to a Cartesian coordinate system where x is along the strong axis of the column (displacement axis), z is in the vertical direction along the length of the column and y is along the weak axis of the column's cross section. Using symmetry of the column cross section, only half the column thickness was modelled (as illustrated in Figure 8) in the interest of computational efficiency. The column models comprised three macroelements, the refined mesh section having 25mm mesh size, the footing and the rest of the column having 50mm mesh size all of which were modelled using 8-noded brick elements. The two other shown macro elements served as loading plates. Rebars were assigned the relevant material and bond properties, a no slip condition was imposed on each bar's both ends. Bars that lie at the plane of symmetry of the column had half the cross-sectional area assigned. Stirrups were assigned perfect connection for bond property. Monotonically increasing lateral displacements were applied in increments of 0.9 mm per step and at constant axial load equal to 10% of the crushing load. Standard Newton-Raphson iteration was used until attainment of nominal strength, then the stepping algorithm was changed to Standard Arc Length.

Modeling Variables

The variables employed in order to capture the difference in behaviour of columns for different corrosion magnitudes were the cross-sectional area of longitudinal and transverse bars, bond strength of longitudinal bars and the size of the concrete cover. For each specimen, longitudinal and transverse bars were assigned the recorded residual area reported by (Vu and Li, 2018), however, due to the lack of evidence regarding the bond strength and the residual (after delamination) concrete cover, the reductions in these parameters were assumed by the authors.

Results

The columns were subjected to a monotonic pushover analysis; the calculated load displacement curves are given in Figure 9 after correction for the second order effects owing to the axial load being translated laterally from its original line of action. Reductions in strength and ultimate drift capacity were clearly captured by the software, however further modelling aspects should be taken into consideration in order to reproduce all aspects of the corroded column condition, such as the location of pitting corrosion, the amount of corrosion of each bar (rather than assuming a uniform mass loss in all bars), the amount of cracking and spalling of the cover prior to testing and the order of magnitude of the reduction in bond strength. However, the model shown is deemed successful in reproducing qualitatively the reported experimental trends, and is quite

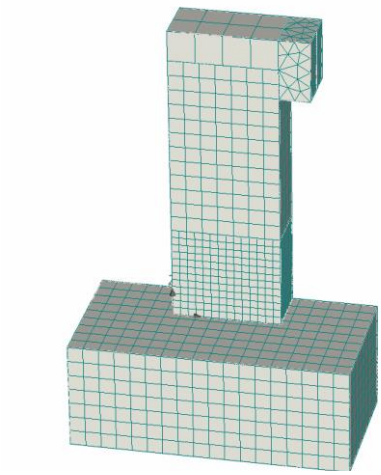

Figure 7 Model of Column U1

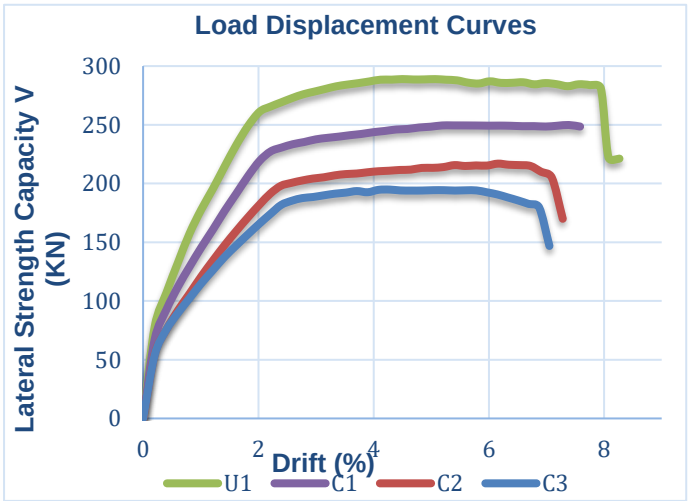

Figure 6 Analytical results of Load-Displacement Curves

consistent with the results of Eq. (6) which summarizes the collective experimental evidence, particularly at larger drifts.

Analytical expressions for shear

Complementary to the parametric equations, the shear capacity of the database columns is examined through existing analytical expressions found in relevant literature for columns in pristine (uncorroded) condition, after necessary modifications to account for geometric area loss of steel and concrete cover. Equation (8) denotes the shear strength of the column in terms of the hierarchy of alternative modes of failure:

$$V_{u,lim} = min\{V_{shear}, V_{anchor}, V_{flex}\} \tag{8}$$

where V_{shear}, V_{anchor} and V_{flex} represent the shear, anchorage and flexural strengths of the column, respectively (i.e., the constant lateral shear force that the column may sustain in order to develop its strength in shear, or the development capacity of its longitudinal reinforcement, or the flexural strength at the critical section at the base). The terms of Eqn. (8) are calculated from the detailing and material properties of the columns using Eqs. (9), (10) and (11) (Pardalopoulos et al, 2017)

$$\mathrm{V_{shear}} = \begin{cases} \mathrm{A_{tr}} \cdot \mathrm{f_{st}} \cdot \frac{\mathrm{d}\cdot(1-\xi)}{\mathrm{s}} \cdot \mathrm{cot\theta_v} & \text{for } \mathrm{v} \le 0.1 \\ \mathrm{v} \cdot \mathrm{tan\alpha} \cdot \mathrm{b} \cdot \mathrm{d} \cdot \mathrm{f_c} + \mathrm{A_{tr}} \cdot \mathrm{f_{st}} \cdot \frac{\mathrm{d}\cdot(1-\xi)}{\mathrm{s}} \cdot \mathrm{cot\theta_v} & \text{for } \mathrm{v} > 0.1 \end{cases} \tag{9}$$

$$\mathrm{V_{anchor}} = \left[\rho_{\mathrm{s,tot}} \cdot \frac{\min\left\{\frac{4\cdot \mathrm{L_a}\cdot \mathrm{f_b}}{\mathrm{D_b}} + \alpha_{\mathrm{hook}}\cdot 50\cdot \mathrm{f_b}; \mathrm{f_y}\right\}}{\mathrm{f_c}} \times (1 - 0.4\xi) + \nu\left(\frac{\mathrm{h}}{\mathrm{d}} - 0.8\xi\right) \right] \cdot \frac{\mathrm{b}\cdot \mathrm{d}^2 \cdot \mathrm{f_c}}{\mathrm{h_{col}}} \tag{10}$$

$$V_{flex} = M/L_s \tag{11}$$

where A_{tr} = area of transverse reinforcement, f_{st} = yield strength of transverse reinforcement, d = effective depth of the column cross section, ξ = normalized depth of the compression zone, s = spacing of stirrups, θ_v = angle of failure plane, v = axial load ratio, α = angle of equivalent compressive strut, b = width of section, f_c = compressive strength of concrete, M = flexural resistance and L_s = shear span of the member (for fixed-fixed column this is half its height).

Pertinent assumptions were made regarding the effect of corrosion in the strength reduction of the reinforcement:

a) In corroded specimens the contribution of the concrete cover was reduced in order to account for cracking sustained due to the dilation caused by the corrosion by-products. For extreme cases of corrosion, the clear cover was reduced to effectively the surface of the transverse reinforcement. For low corrosion levels however, the cover was found to be partly contributing at least in some specimens; one of the major causes for this range is the variety of the methods for imposing accelerated corrosion in the tests, which led to the creation of oxides with different specific densities. This aspect requires further study.

b) Mass loss, average area loss and maximum area loss were extracted where reported. In cases where such information was not available, the corresponding values were estimated using the trend lines supported by the existing data, using interpolation (see Fig. 10). The area of the reinforcing bars affected by corrosion was reduced by the relevant average area loss parameter and used as such in the above Eqs. (9-11).

Results obtained from the analytical calculations were compared with the experimental values reported in the cited literature and the ratios of calculated lateral load resistance normalized by the experimental estimate are summarized in Figs. 11 and 12. Flexural failures were observed in the majority of the specimens (denoted in blue) whereas shear failures (denoted in red) were observed in a small number of the specimens. One case was denoted as green to identify a mixed flexural – shear mode of failure reported by (Vu and Li, 2018). It is noteworthy here that the calculated shear and flexural capacities resulted in similar values.

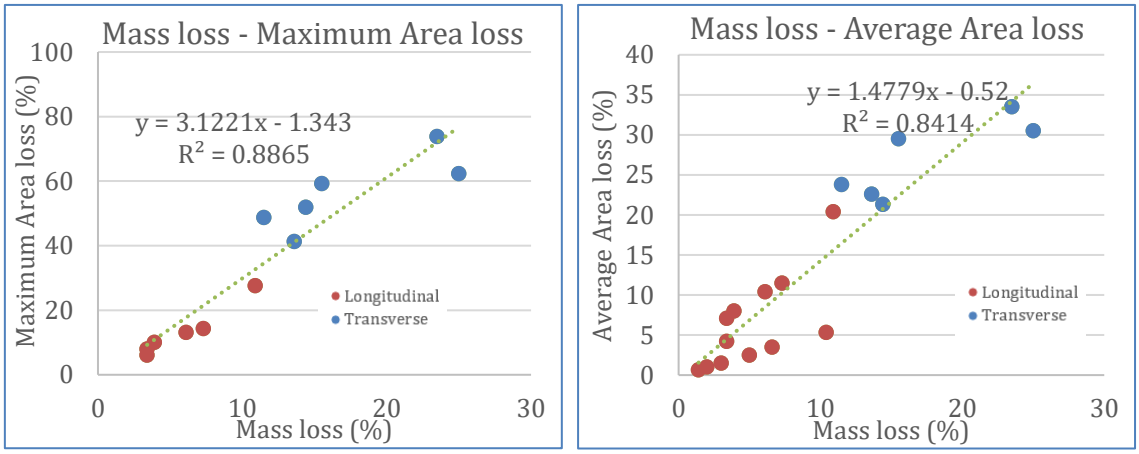

Figure 10 Correlations between maximum area loss – mass loss (left) and average area loss – mass loss (right).

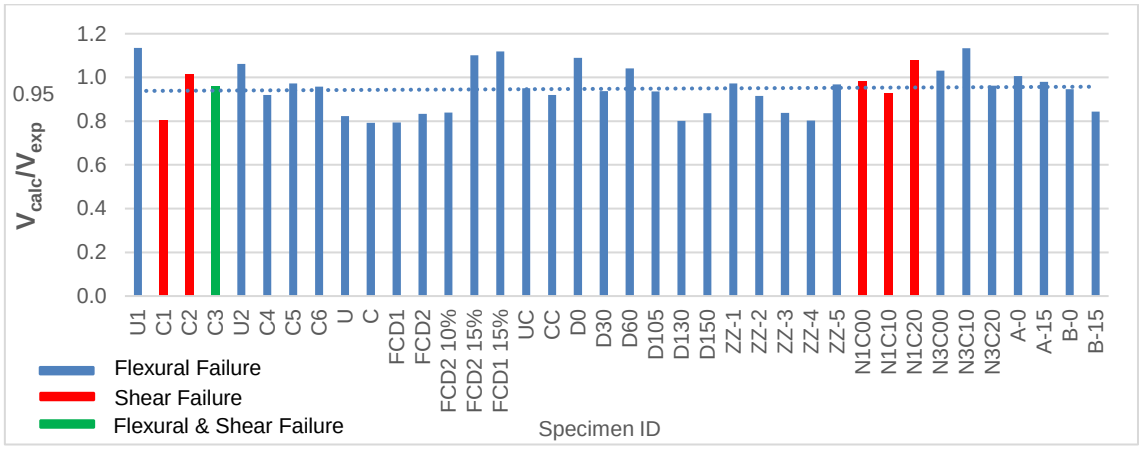

Figure 11 Ratio between calculated shear strength to experimental shear strength.

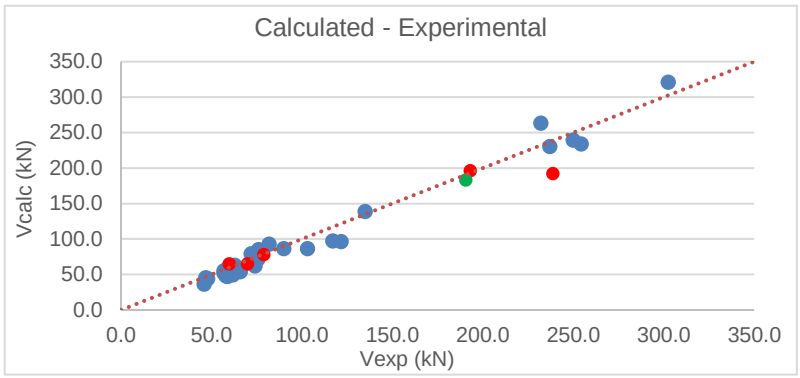

Figure 12 Correlation between calculated and experimental shear strength.

Conclusion

In the current study, a thorough examination on experimental investigations of corrosion damage was conducted, with the aim of providing a predictive framework for evaluating deteriorated structures. Evidence from the accumulated database reveal a pattern of reduction in the overall strength and ductility of the reinforcement (owing to mass losses), and a significant decrease in the lateral strength and drift capacity of the afflicted structural members; expressions quantifying this decrease were formulated in this regard. Parallel finite element analysis and analytical calculations affirm the observed patterns in the progressive corrosion damage. Further investigation is to be implemented in order to formulate applicable expressions to assess corrosion damaged structures.

Appendix

Corroded Columns Database

Project	Specimen name	B (mm)	H (mm)	Long. Reinf.	Trans. Reinf.	Axial Load (%)	Current Density (μA/cm²)	% mass loss
(Vu and Li, 2018).	U1	350	350	8 T 20	Φ8 @ 50	10	500	0
	C1	350	350	9 T 20	Φ8 @ 50	10	500	3.4
	C2	350	350	10 T 20	Φ8 @ 50	10	500	6.1
	C3	350	350	11 T 20	Φ8 @ 50	10	500	10.9
	U2	350	350	12 T 20	Φ8 @ 50	25	500	0
	C4	350	350	13 T 20	Φ8 @ 50	25	500	3.4
	C5	350	350	14 T 20	Φ8 @ 50	25	500	3.9
	C6	350	350	15 T 20	Φ8 @ 50	25	500	7.3
(Apostolopoulos, et al, 2019)	U	300	300	4 T 16	Φ8 @ 250	12	-	0
	C	300	300	4 T 16	Φ8 @ 250	12	-	17
(Rajput and Sharma, 2018).	FCD1	300	300	8 T 16	Φ10 @ 75	35	200	0
	FCD2	300	300	8 T 16	Φ10 @ 75	35	200	0
	FCD2	300	300	8 T 16	Φ10 @ 75	35	200	10
	FCD2	300	300	8 T 16	Φ10 @ 75	35	200	14.86
	FCD1	300	300	8 T 16	Φ10 @ 75	35	200	15.33
(Li, Gong and Wang, 2009).	A0	200	200	4 T 14	Φ8 @ 100	35	100	0
	B3	200	200	4 T 14	Φ8 @ 100	35	100	16.8
(Meda *et al.*, 2014).	UC	300	300	4 T 16	Φ8 @ 300	22	5000	0
	CC	300	300	4 T 16	Φ8 @ 300	22	5000	20
(Ma, et al 2012)	C0-15	D = 260		6 T 16	Φ8 @ 100	15	-	0
	C9-15	D = 260		6 T 16	Φ8 @ 100	15	-	9.5
	C0-25	D = 260		6 T 16	Φ8 @ 100	25	-	0
	C4-25	D = 260		6 T 16	Φ8 @ 100	25	-	4.1
	C9-25	D = 260		6 T 16	Φ8 @ 100	2	-	9.7
	C0	D = 260		6 T 16	Φ8 @ 100	40	-	0
	C9-40	D = 260		6 T 16	Φ8 @ 100	40	-	9.3
(Yuan, et al. 2017)	D0	D = 400		10 T 16	Φ8 @ 70	13	300	0
	D30	D = 400		10 T 16	Φ8 @ 70	13	300	4.57
	D60	D = 400		10 T 16	Φ8 @ 70	13	300	8.69
	D105	D = 400		10 T 16	Φ8 @ 70	13	300	17.59
	D130	D = 400		10 T 16	Φ8 @ 70	13	300	28.52
	D150	D = 400		10 T 16	Φ8 @ 70	13	300	30.71
(Yang *et al.*, 2016).	ZZ-1	210	210	4 T 18	Φ6 @ 90	18	610	0
	ZZ-2	210	210	4 T 18	Φ6 @ 90	18	610	5.1
	ZZ-3	210	210	4 T 18	Φ6 @ 90	18	610	8.3
	ZZ-4	210	210	4 T 18	Φ6 @ 90	18	610	13.25
	ZZ-5	210	210	4 T 18	Φ6 @ 90	18	610	16.8
(Li *et al.*, 2018).	N1C00	300	300	6 T 22	Φ8 @ 100	10	300-1000	0
	N1C10	300	300	6 T 22	Φ8 @ 100	10	300-1000	6.92
	N1C20	300	300	6 T 22	Φ8 @ 100	10	300-1000	13.47
	N3C00	300	300	6 T 22	Φ8 @ 100	30	300-1000	0
	N3C10	300	300	6 T 22	Φ8 @ 100	30	300-1000	7.2
	N3C20	300	300	6 T 22	Φ8 @ 100	30	300-1000	17.7
(Liu and Li, 2018).	A-0	D = 300		8 T 12	Φ8 @ 80	30	829.4	0
	A-15	D = 300		8 T 12	Φ8 @ 80	30	829.4	14.55
	B-0	D = 300		8 T 14	Φ8 @ 80	30	829.4	0
	B-15	D = 300		8 T 14	Φ8 @ 80	30	829.4	15.92

References

Almusallam, A. A. *et al.* (1996) 'Effect of reinforcement corrosion on bond strength', *Construction and Building Materials*. Elsevier, 10(2), pp. 123–129. doi: 10.1016/0950-0618(95)00077-1.

Almusallam, A. A. (2001) 'Effect of degree of corrosion on the properties of reinforcing steel bars', *Construction and Building Materials*. Elsevier, 15(8), pp. 361–368. doi: 10.1016/S0950-0618(01)00009-5.

Alonso, C. *et al.* (1998) 'Factors controlling cracking of concrete affected by reinforcement corrosion', *Materials and Structures*. Kluwer Academic Publishers, 31(7), pp. 435–441. doi: 10.1007/BF02480466.

Apostolopoulos, C. A. (2007) 'Mechanical behavior of corroded reinforcing steel bars S500s tempcore under low cycle fatigue', *Construction and Building Materials*. Elsevier, 21(7), pp. 1447–1456. doi: 10.1016/J.CONBUILDMAT.2006.07.008.

Apostolopoulos, C. A. and Papadakis, V. G. (2008) 'Consequences of steel corrosion on the ductility properties of reinforcement bar', *Construction and Building Materials*. Elsevier, 22(12), pp. 2316–2324. doi: 10.1016/J.CONBUILDMAT.2007.10.006.

Apostolopoulos, C., Drakakaki, A. and Basdeki, M. (2019) 'Seismic assessment of RC column under seismic loads', *International Journal of Structural Integrity*. Emerald Publishing Limited , 10(1), pp. 41–54. doi: 10.1108/IJSI-02-2018-0013.

Cervenka Consulting (2007) 'ATENA Program Documentation'. Prague, Czech Republic.

Du, Y. G., Clark, L. A. and Chan, A. H. C. (2005) 'Residual capacity of corroded reinforcing bars', *Magazine of Concrete Research*. Thomas Telford Ltd , 57(3), pp. 135–147. doi: 10.1680/macr.2005.57.3.135.

Fernandez, I., Bairán, J. M. and Marí, A. R. (2015) 'Corrosion effects on the mechanical properties of reinforcing steel bars. Fatigue and σ–ε behavior', *Construction and Building Materials*. Elsevier, 101, pp. 772–783. doi: 10.1016/J.CONBUILDMAT.2015.10.139.

François, R., Khan, I. and Dang, V. H. (2013) 'Impact of corrosion on mechanical properties of steel embedded in 27-year-old corroded reinforced concrete beams', *Materials and Structures*. Springer Netherlands, 46(6), pp. 899–910. doi: 10.1617/s11527-012-9941-z.

Li, D. *et al.* (2018) 'Influence of Non-uniform corrosion of steel bars on the seismic behavior of reinforced concrete columns', *Construction and Building Materials*. Elsevier, 167, pp. 20–32. doi: 10.1016/J.CONBUILDMAT.2018.01.149.

Li, J., Gong, J. and Wang, L. (2009) 'Seismic behavior of corrosion-damaged reinforced concrete columns strengthened using combined carbon fiber-reinforced polymer and steel jacket', *Construction and Building Materials*. Elsevier, 23(7), pp. 2653–2663. doi: 10.1016/J.CONBUILDMAT.2009.01.003.

Liu, X. and Li, Y. (2018) 'Experimental study of seismic behavior of partially corrosion-damaged reinforced concrete columns strengthened with FRP composites with large deformability', *Construction and Building Materials*. Elsevier, 191, pp. 1071–1081. doi: 10.1016/J.CONBUILDMAT.2018.10.072.

Lu, C. *et al.* (2016) 'Mechanical properties of corroded steel bars in pre-cracked concrete suffering from chloride attack', *Construction and Building Materials*, 123(123), pp. 649–660. doi: 10.1016/j.conbuildmat.2016.07.032.

Ma, Y., Che, Y. and Gong, J. (2012) 'Behavior of corrosion damaged circular reinforced concrete columns under cyclic loading', *Construction and Building Materials*. Elsevier, 29, pp. 548–556. doi: 10.1016/J.CONBUILDMAT.2011.11.002.

El Maaddawy, T. A. and Soudki, K. A. (2003) 'Effectiveness of Impressed Current Technique to Simulate Corrosion of Steel Reinforcement in Concrete', *Journal of Materials in Civil Engineering*, 15(1), pp. 41–47. doi: 10.1061/(ASCE)0899-1561(2003)15:1(41).

Mangat, P. S. and Elgarf, M. S. (1999) 'Bond characteristics of corrding reinforcement in concrete beams', *Materials and Structures*. Kluwer Academic Publishers, 32(2), pp. 89–97. doi: 10.1007/BF02479434.

Meda, A. *et al.* (2014) 'Experimental evaluation of the corrosion influence on the cyclic behaviour of RC columns', *Engineering Structures*. Elsevier, 76, pp. 112–123. doi: 10.1016/J.ENGSTRUCT.2014.06.043.

Pardalopoulos, S. I., Pantazopoulou, S. J. and Lekidis, V. A. (2017) 'Simplified method for rapid seismic assessment of older R.C. buildings'. doi: 10.1016/j.engstruct.2017.10.052.

Rajput, A. S. and Sharma, U. K. (2018) 'Corroded reinforced concrete columns under simulated seismic loading', *Engineering Structures*. Elsevier, 171, pp. 453–463. doi: 10.1016/J.ENGSTRUCT.2018.05.097.

Stanish, K., Hooton, R. D. and Pantazopoulou, S. J. (1999) 'Corrosion Effects on Bond Strength in Reinforced Concrete', *ACI Structural Journal*, 96(6), pp. 915–921. doi: 10.14359/765.

Tastani, S. P. and Pantazopoulou, S. J. (2007) 'Behavior of Corroded Bar Anchorages', *ACI Structural Journal*, 104(6), pp. 756–766. doi: 10.14359/18958.

Vu, N. S. and Li, B. (2018) 'Seismic Performance of Flexural Reinforced Concrete Columns with Corroded Reinforcement', *ACI Structural Journal*, 115(5), pp. 1253–1266. doi: 10.14359/51702372.

Yang, S.-Y. *et al.* (2016) 'Experimental research on hysteretic behaviors of corroded reinforced concrete columns with different maximum amounts of corrosion of rebar', *Construction and Building Materials*. Elsevier, 121, pp. 319–327. doi: 10.1016/J.CONBUILDMAT.2016.06.002.

Yuan, W., Guo, A. and Li, H. (2017) 'Experimental investigation on the cyclic behaviors of corroded coastal bridge piers with transfer of plastic hinge due to non-uniform corrosion', *Soil Dynamics and Earthquake Engineering*. Elsevier, 102, pp. 112–123. doi: 10.1016/J.SOILDYN.2017.08.019.

Zhang, W. *et al.* (2012) 'Tensile and fatigue behavior of corroded rebars', *Construction and Building Materials*. Elsevier, 34, pp. 409–417. doi: 10.1016/J.CONBUILDMAT.2012.02.071.

Zhao, Y. *et al.* (2013) 'Bond behaviour of normal/recycled concrete and corroded steel bars', *Construction and Building Materials*. Elsevier, 48, pp. 348–359. doi: 10.1016/J.CONBUILDMAT.2013.06.091.

Zhu, W. and François, R. (2014) 'Experimental investigation of the relationships between residual cross-section shapes and the ductility of corroded bars', *Construction and Building Materials*, 69(69), pp. 335–345.